CHAPTER VIII
SYNERGY BETWEEN Ru AND Ni ON Ru-Ni/HMOR CATALYSTS AND ITS PARTICULAR INFLUENCES ON TIRE PYROLYSI PRODUCTS

8.1 Abstract

Pyrolysis of waste tire with RuNi/HMOR catalyst was investigated. The seven studied catalysts having different α, α = Ru/(Ru + Ni), were prepared by successive impregnation technique started with Ru. All prepared catalysts strongly influence the yield and nature of pyrolysis products, and their catalytic activity depend on the metal composition of the catalyst. Particularly, significant synergistic effects were observed on both aromatic reduction and naphtha production in the tire-derived oil obtained from catalytic pyrolysis with bimetallic catalysts. And the synergistic effect was found to be strongly contingent upon the metal composition of the bimetallic catalyst, α. The synergistic effect first increased with increasing α, peaked up at α = 0.36, and then decreased with higher α. It was evident that the close interaction reaction between ruthenium and nickel, leading to the formation of bimetallic particles, was the cause for the observed synergistic effects.

8.2 Introduction

The increasing amount of waste tire generated annually undoubtedly emerges as a serious environmental issue. At the same time, the gradual depletion of petroleum reserves has created interest in finding the alternative source of energy. Therefore, the pyrolysis of waste tire has been receiving renewed attention since its products have high potentials to be used, particularly the oil [1]. However, the use of pyrolytic oil as fuel is limited due to its high content of aromatics, particularly poly- and polar-aromatics [2].

Recently, it was reported that among noble metals (Ru, Re, Rh, Pt) supported on HMOR catalysts, Ru based catalyst showed the best performance in waste tire pyrolysis for aromatic reduction and light oil production simultaneously

[3]. On the other hand, the introduction of a second metal can influence the property of the first dispersed metal due to the formation of metallic clusters [4]. Moreover, bimetallic catalysts may exhibit superior activity, selectivity, and deactivation resistance than their corresponding monometallic samples [5,6].

The bimetallic RuNi catalyst has been widely investigated [7-11]. And generally it was found that this bimetallic catalyst exhibited much higher activity and selectivity than their corresponding monometallic samples. Crisafulli et al. reported that the bimetallic Ni-Ru supported on SiO_2 shows much higher activity and stability than the Ni/SiO_2 sample [8]. Meanwhile, to the best of our knowledge, no study on bimetallic Ru-Ni supported on HMOR zeolite in the catalytic pyrolysis of waste tire has been reported in literatures.

The aim of the present study is to investigate the catalytic activity of RuNi/HMOR catalyst for the conversion of waste tire. Therefore, a series of RuNi/HMOR was prepared by successive impregnation technique, and their catalytic activity for waste tire pyrolysis were studied and discussed in relation with their characterizations.

8.3 Experimental

8.3.1 Catalyst Preparation

Mordenite (MOR, H-form, SiO_2/Al_2O_3 mole ratio = 19, surface area = 380 m^2/g) zeolite supplied by the TOSOH (Singapore) was first calcined in air at 500°C for 3 hours. Ru ($RuCl_3$, FLUKA) and Ni ($Ni(NO_3)_2$, ALDRICH) were then loaded using successive impregnation techniques. Ruthenium was first loaded, followed by drying in oven at 110°C for 3 hours, and then Ni was introduced into the sample. A total metal loading of 2% was kept constant in all samples. And α ratio, defined as Ru/(Ru + Ni) in weight, was varied from 0, 0.25, 0.36, 0.50, 0.64, 0.75, to 1. Therefore, from this point the sample will be denoted by its α value. After impregnation with metallic precursors, the samples were dried in oven for 3 hours at 110°C, and calcined at 500°C for another 3 hours. Next, they were pelletized, ground, and then sieved to specific particle sizes of 400–425 μm. Prior to catalytic activity measurement, the catalysts were reduced at 500°C by H_2 for 3 hours.

8.3.2 Catalyst Characterization

The XRD patterns were recorded by a Riguku D/Max 2200H apparatus with a scanning speed of 0.5 degrees/min and 2θ from 5 degrees to 60 degrees. The Raman spectra were measured with a Perkin-Elmer GX Raman FT-IR apparatus equipped with a Nd:YAG (1064 nm) laser and an InGaAs detector. For each spectrum, an average of 10–50 scans were obtained with a laser power the 40–300 mW in the 1000 cm^{-1} – 20 cm^{-1} range with the 4 cm^{-1} – 2 cm^{-1} resolution. Diffuse reflectance UV-visible spectroscopic measurements were recorded on a Shimadzu UV-2550 spectrometer fitted with an ISR-2200 integrating sphere attachment from 200-600nm reference to $BaSO_4$.

The amounts of the Ru and Ni on the support were determined by the Inductively Coupled Plasma (ICP) technique using a Perkin Elmer Optima 4300 PV machine. The surface area (BET) and pore volume of the studied catalysts were characterized by N_2 physical adsorption using the Sorptomatic 2900 equipment.

Hydrogen and CO chemisorption at room temperature of the reduced samples were carried out in a chemisorption system equipped with a TCD, after the pre-treatment of sample at 150°C (10°C/min) for 1 hour, under a flow of helium.

Temperature-programmed techniques including TPR, TPD, and TPO were conducted using a TPD/TPR Micromeritics 2900 apparatus. For TPD-NH_3, approximately 0.1g of sample was first pretreated in He at 550°C for 30 minutes. Then, the system was cooled to 100°C, and the NH_3 adsorption was performed using NH_3/N_2 for 1.5 hours followed by the introduction of He for 30 minutes at 100°C to remove the physically adsorbed NH_3. Finally, the system was cooled to 50°C, and then the temperature program desorption was started from 50°C to 600°C with the heating rate of 5°C/min. H_2-TPR profiles of the calcined samples were recorded from room temperature (30°C) to 600°C with the heating rate of 10°C/min using 5% H_2/N_2 after pretreatment of the samples at 150° under a helium flow (30ml/min) for 30 minutes. Temperature program oxidation (TPO) was performed from room temperature to 900°C (10°C/min), and the final temperature was held for 30 minutes. The amount of coke was then determined from the area under the curve and calculated by the software supplied with the machine.

8.3.2 Pyrolysis of Waste Tire

The detail of pyrolysis process was described elsewhere [12]. Briefly, a tire sample was pyrolyzed in the lower zone (500°C), and then the evolved product was carried by a nitrogen flow to the upper zone of the reactor packed with a catalyst (350°C). The product was next passed through an ice-salt condensing system to separate incondensable compounds from the liquid product. The solid and liquid products were weighed to determine the product distribution. The amount of gas was then determined by mass balance. The liquid product was first dissolved in n-pentane to precipitate asphaltenes. Then, a Varian CP 3800 Simulated Distillation Gas Chromatograph (SIMDIST GC) equipped with FID was used to analyze the obtained maltenes according to the ASTM D2887 method for simulated true boiling point curves. Finally, the maltenes was analyzed for its compositions in terms of hydrocarbon types, including saturates, mono-, di-, poly- and polar-aromatics by means of liquid adsorption chromatography [13].

8.4 Results

8.4.1 Catalyst Characterization

Figure 8.1 shows the XRD patterns of the bimetallic samples, their corresponding mono-metallic ones and HMOR zeolite. It can be seen that the introduction of metal leads to a slight decrease in the crystallinity of the parent zeolite, as deduced from the reduction in the intensity of the peaks at 2θ of 22.5°, 26°, and 28°. Apart from these crystallinity reductions, neither peak of Ru and/or Ni species nor any new phase is observed in the XRD patterns of all samples. The disappearance of the peaks corresponding to Ni and Ru species is possibly due to the low amount of metal loading used (2%wt).

The chemical compositions of all the prepared catalysts determined by ICP are presented in Table 8.1. Accordingly, the amount of metals loaded is consistent with the targeted value. Table 8.1 also summarizes several textural properties obtained from nitrogen adsorption/desorption analysis. The incorporation of metals decreases not only surface area but also pore volume in all samples. These observations together with the XRD results suggest the occurrence of metal diffusion into the zeolite channels. It is also worth mentioning that Ru/HMOR (α = 1) has

considerable low pore volume and surface area as compared to all the other metal-supported catalysts.

Table 8.1 Physical-chemical properties of prepared catalysts

Catalyst	Metal content (wt%)		Surface area (m^2/g)	Pore volume (cm^3/g)	Spent Catalysts		CO/H	NH_3 uptakes (mmol/g)	
	Ni	Ru			Coke (wt%)	S (wt%)		M + S	Total
α = 0	2.09	-	363.7	0.21	38.5	3.2	2.19	2.27	3.44
α = 0.25	0.48	1.51	365.5	0.21	22.9	0.8	1.56	1.56	2.80
α = 0.36	0.71	1.35	365.1	0.20	17.7	0.5	2.08	2.64	3.95
α = 0.50	1.05	1.02	367.7	0.21	21.3	0.7	1.25	1.45	2.82
α = 0.64	1.32	0.73	371.9	0.22	26.1	1.5	1.07	0.91	2.88
α = 0.75	1.49	0.52	364.3	0.23	24.4	1.3	0.98	1.07	3.59
α = 1.0	-	2.04	318.8	0.17	27.8	1.9	0.79	0.72	3.42

TPR profiles of the prepared catalysts are shown in Figure 8.2. Prior to performing TPR with metal supported samples, the unloaded zeolite was subjected to test for its H_2 consumption. The result (not shown) indicates that the unloaded zeolite does not consume hydrogen under the TPR conditions. In case of monometallic Ni sample (α = 0), a broad intense and asymmetric peak with a maximum at ~ 490°C, and a small shoulder at 600°C is observed (Figure 8.2B). Ru sample (α = 1) shows two reduction peaks: a sharp and symmetric one at ~ 190°C and another broad peak at about ~330°C (Fig. 8.2A). And, this broad peak (330°C) of Ru sample decreases, and then disappears with decreasing α (increasing Ni content). The observed phenomenon could be ascribed to various reasons. The first reason is that this peak is probably overlapped by the big broad peak of Ni species at ~ 500°C. Another possible reason is that there likely exists certain interaction between Ru and Ni [14]. Moreover, for all RuNi samples, the peak at 190°C shifts toward higher temperatures, whereas the peak at ~ 500°C shifts toward lower temperatures, indicating the chemical interaction between Ru and Ni. The shifts are probably due to the easier reducibility of ruthenium, activating hydrogen; thus, favoring the reduction of nickel species by a spillover effect [8,15]. These observations suggest

the formation of bimetallic particles on RuNi samples [8]. And, the highest shift is observed over the $\alpha = 0.36$ sample (Figures 8.2A and B).

In order to further study the topology of the prepared samples, their DRUV spectra were recorded, and the obtained results are presented in Figure 8.3. DRUV has been widely used to identify the phase of materials [16-18]. As seen in the figure, there emerges a new single peak with maximum at about 208 nm in all RuNi samples. This peak might result from the combination of the peak of Ni at 210 nm and the peaks of Ru at 205 nm and 208 nm. In fact, this phenomenon is observed the most clearly with $\alpha = 0.36$, which is well consistent with TPR results (Figure 8.2). These results might further confirm the existence of the close interaction between Ni and Ru, making the assumption on the formation of bimetallic particles possible. The Raman spectra of the studied catalysts are depicted in Figure 8.4. This figure indicates that the addition of metal did not affect the structure of the support, but changed the intensity of the peak of support. No difference between the bimetallic samples is found from the Raman spectra except for the intensity.

As revealed from TPR and DRUV analysis, bimetallic particles are possibly present on the RuNi samples. Therefore, it might not be accurate to determine the metal dispersion based on the assumption of the surface composition. Thus, the H_2 and CO chemisorption were performed to qualitatively estimate the metal dispersion by CO/H ratio [19] for the prepared catalysts. The obtained results are given in Table 8.1. Hydrogen is well-known to chemisorb dissociatively on the active site, and its chemisorption nature is independent on how a metal is dispersed. On the other hand, the metal dispersion markedly affects the nature of CO adsorption. CO can approach an active site from all the directions for a highly-dispersed metal catalyst, and more than one molecule of CO may be chemisorbed on an active site [19]. Therefore, for a highly-dispersed metal catalyst, the CO/H adsorption ratio ranges between 2 and 3. In contrast, for a poorly-dispersed metal catalyst, one CO molecule is shared by two active sites, resulting in a CO/H uptake ratio of less than unity. However, for a moderately dispersed catalyst, the ratio is close to unity [19]. Based on these understandings and from the CO/H ratio values presented in Table 8.1, one can deduce that the metals are highly dispersed on the samples with $\alpha = 0$ and $\alpha = 0.36$, and moderately dispersed in all the other bimetallic samples, and the

least dispersed in Ru sample (α = 1). This lowest dispersion of ruthenium monometallic sample probably causes its lowest pore volume and surface area (Table 8.1).

The concentration and distribution of acid sites of the prepared catalysts were analyzed by TPD-NH_3, and the obtained results are presented in Figure 8.5 and Table 8.1. The HMOR zeolite gives two peaks with maxima at around 200°C and 500°C. The presence of Ni insignificantly influences the TPD profile of the support. Meanwhile, the incorporation of Ru causes a shift of the peak at ~ 510°C to lower temperatures, and also an emergence of a new peak at approximate 230°C, possibly due to the metal-support interaction [10] and/or the high tendency of ruthenium to adsorb ammonia [20]. In the spectra of bimetallic samples, this new peak (of ruthenium) decreases, and the shift of the peak at 510°C is also lessened with increasing Ni content. Moreover, the desorption temperature can be used to classify the type of acid sites as weak (< 250°C), medium (250°C - 350°C), and strong (> 350°C). And, the distribution and concentration of acid sites for all samples, as determined by the area under the peaks, are given in Table 8.1. The highest total acidity and the highest medium and strong (M+S) acidity are observed at α = 0.36.

The TPO profiles (not shown here) of the spent catalysts show two peaks with the maxima located at around 300°C and 500°C. Quantitative analysis shows that there is some considerable amount of coke on each spent catalyst. The presence of metallic sites, favoring hydrogen transfer and coke forming reaction [21,22], might be the reason for the relatively-high coke formation. Interestingly, a higher amount of coke is detected on the spent monometallic catalysts than all RuNi samples ones, and the spent Ni sample (α = 0) contains the highest amount of coke. This result is consistent with those reported in literatures that nickel in the metallic state is responsible for coke formation in a large range of catalyst and processes [21,23]. And, for all studied samples the order of coke formation can be summarized as follows: $\alpha = 0 > \alpha = 1 > \alpha = 0.64 > \alpha = 0.75 > \alpha = 0.25 > \alpha = 0.50 > \alpha = 0.36$. The spent catalysts were also analyzed for its sulfur content by elemental analysis, and the obtained results are also given in Table 8.1. Interestingly, the order of sulfur content of a spent catalyst is well in line with its amount of coke. From these results, it can be concluded that the monometallic Ru sample exhibits better coke resistance

and sulfur tolerance than the monometallic Ni, but lower than all bimetallic samples.

8.4.2 Catalytic activity measurement.

The influences of α ratio on the products obtained from the catalytic pyrolysis of waste tire are present in Figures 8.6, 8.7, and 8.8. Figure 8.6 illustrates the yields of pyrolysis products for all prepared catalysts. The data of non-catalytic case are also given for comparison purpose. Accordingly, the yield of solid product is similar in all runs (~ 48%), which is due to the fact that same pyrolysis conditions were employed and the tire was reported to completely decomposed at 500°C [12]. The presence of catalysts, as expected, increases the yield of gaseous product at the expense of oil yield. Moreover, the yields of pyrolysis products strongly depend on the metal composition of the catalysts. The yield of gaseous product increases with the incorporation of the second metal, then peaks up at $\alpha = 0.36$, and subsequently decreases with higher α values. The increase in gas yield reflects higher cracking activity of a catalyst in general.

Figures 8.7A and 8.7B present the concentration of poly-, polar- and total aromatics in the tire-derived oils for all catalysts. Thermal pyrolysis produces the oil comprising of about 8, 12, and 47 wt% of poly-, polar- and total aromatics, respectively. Thus, the presence of catalysts drastically decreases the concentration of poly- and polar-aromatics (Figure 8.7A). Total aromatics in oils also decreased, and the degree of total aromatic reduction strongly depends on the value of α. The total aromatics first decreases with α, reaches a minimum at $\alpha = 0.36$, and then increases with further increasing in α. In addition, the activity of RuNi catalysts on aromatic reduction is higher than their corresponding physical mixture of individual catalysts, indicating the synergistic effect, which also can be observed from poly- and polar-aromatic reduction (Figure 8.7A).

Additionally, the metal composition also strongly affects the content of petroleum fractions in the derived oils. Naphtha fraction (boiling point < 200°C) can be used as an indicator for the high cracking ability of a catalyst. The higher content of naphtha, the lighter oil is obtained. It is also worthy noted that naphtha is among the most valuable fractions commercially. As seen in Figure 8.8, the activity for light oil production increases with the incorporation of Ni, reaches a maximum when $\alpha = 0.36$, and then decreases with higher α. These results show a significant

synergistic effect of incorporation of Ni on the Ru catalyst, which has the impact on the production of naphtha in the derived oil. Summarily, the important synergy can be observed from both aromatic reduction and naphtha production with the use of bimetallic RuNi catalysts, and the degree of synergy depends on the value of α.

8.5 Discussion

8.5.1 General

As revealed from the liquid analysis, a high concentration of aromatics, particularly the polycyclic aromatics in oil for non-catalytic pyrolysis, was observed. Meanwhile, it was shown that the presence of metal clusters might promote the conversion of these hydrocarbons [24] possibly to the (partial) hydrogenated compounds, making them more reactive for cracking over acidic sites. Consequently, the use of RuNi catalysts decreases the concentrations poly- and polar-aromatic compounds in the derived oil, and simultaneously produces lighter oil and higher yields of gas products (Figures 8.7 and 8.6). However, it should be noted that the considerable high amount of coke detected on the spent catalysts might also particularly be the cause for the reduction of polycyclic aromatics in the derived oil, as proposed in [26] and the references therein.

On the other hand, according to Figures 8.6-8.8, it can be concluded that Ru/HMOR exhibits higher activity for waste tire pyrolysis than Ni/HMOR, despite the fact that higher metal dispersion as well as concentration of medium and strong acid sites are observed in the later catalyst (Table 8.1). Therefore, the higher activity of Ru/HMOR can be ascribed to its intrinsic nature that can effectively catalyze hydrogenation reactions, and particularly exhibits high sulfur-tolerance [3,27]. Ru-based catalyst was also reported as the best metal among Ru, Rh, Re, and Pt catalysts for waste tire conversion [3]. Finally, all bimetallic catalysts are better than their corresponding monometallic ones.

8.5.2 Synergy

It can be seen from Figures 8.7 and 8.8 that significant synergistic effects are observed on both aromatic reduction and naphtha production with all prepared bimetallic catalysts. For the ease of analysis, the factor of synergy (ζ) for

naphtha production (ζ_N) and for aromatic reduction (ζ_A) are then defined as shown in the following equations:

$$\zeta_N = \frac{N(RuNi)_\alpha}{\alpha N(Ru) + (1-\alpha)N(Ni)} \quad \text{, and} \quad \zeta_A = \frac{\alpha A(Ru) + (1-\alpha)A(Ni)}{A(RuNi)_\alpha}$$

where N is naphtha content in oil (wt%); A is total aromatic content in oil (%wt). The naphtha (aromatic) content in the oil obtained from pyrolysis using a physically-mixed monometallic Ru and Ni catalyst at any α was calculated based on the naphtha (aromatic) content in the oil obtained from pyrolysis using each individual catalyst. Similar calculation to observe the synergistic effects was reported in [28].

Table 8.2 Factor of synergy (ζ) of all prepared catalysts

ζ \ α	0	0.25	0.36	0.50	0.64	0.75	1.0
Naphtha production (ζ_N)	1.00	1.18	1.55	1.29	1.11	1.20	1.00
Aromatic reduction (ζ_A)	1.00	1.26	1.57	1.29	1.19	1.00	1.00

Table 8.2 summarizes the factors of synergy of all prepared catalysts for naphtha production and aromatic reduction. Interestingly, the values of ζ for naphtha production and aromatic reduction are comparable at almost all α values. In addition, for both cases, ζ first increases, reaches a maximum at $\alpha = 0.36$, and then decreases with further increasing α. And, also from the table, the order of the synergy is: $\alpha = 0.36 > \alpha = 0.50 > \alpha = 0.25 > \alpha = 0.64 > \alpha = 0.75$. One can realize that this order is similar to the order of the degree of ruthenium-nickel interaction (Figure 8.2). At $\alpha = 0.36$, the highest value of ζ is achieved in both cases, indicating that this is the most effective composition for the production of tire-derived oil that contains high naphtha and low aromatic contents.

It has been proposed frequently that many reactions, such as cracking,

isomerization, hydrogen transfer, aromatization, and alkylation, simultaneously occur during the catalytic pyrolysis of waste tire [12,29]. Therefore, the product selectivity depends on the dominance of one reaction over the others. However, it is reasonable that cracking reaction is mainly responsible for the selectivity to light product, whereas hydrogen transfer and/or aromatization are responsible for the type of products. And the extent of catalytic cracking reaction depends on many factors such as pore diameter, pore volume, but greatly depends on the density of strong acid sites [30,31]. On the other hand, it is noted that hydrogenation over metal sites is favored at low temperature due to its exothermic characteristic [32]. Therefore, the high temperature (350°C) employed in the present study is thermodynamically unfavored for this reaction. As a consequence, the degree of hydrogenation (over metal sites) probably depends on the reactions, that convert hydrogenated products (to shift the equilibrium), like ring-opening and cracking (mainly over acid sites). Moreover, it is well accepted that the cracking of an aromatic (over acid sites) should require an initial hydrogenation (over metal sites). Also, it should be noted that Ru itself was proven to have ability to convert poly- and polar-aromatics into lighter compounds, enhancing naphtha production from pyrolysis of waste tire [24]. From these understandings, the synergistic effects observed over bimetallic samples can be ascribed to the interaction between ruthenium and nickel, which leads to the enhancement of ruthenium performance as well as better coke resistance and sulfur tolerance. Consequently, the highest activity of $\alpha = 0.36$ sample can be ascribed to its strongest metal-metal interaction. And, although $\alpha = 0.25$ has a better metal dispersion than $\alpha = 0.50$, while their acidic properties are similar (Table 8.1), it has lower ζ. This can be explained taking into account the fact that there exist a stronger metal-metal interaction in the $\alpha = 0.50$ sample (Figure 8.2), resulting in its better coke resistance and sulfur tolerance (Table 8.1).

The low activity of Ni sample (Figures 8.6, 8.7, and 8.8), despite its highest metal dispersion and high S+M acid density, can be explained by several approaches. The intrinsic nature of nickel that can form carbonyl species with CO [19], resulting in a high CO/H ratio. Additionally, the high metal dispersion of this metal can not compensate its low coke resistance and sulfur tolerance, since considerable high amounts of coke and sulfur are detected on the spent Ni/HMOR.

(Table 8.1). The low coke resistance of Ni-based catalysts was reported in the literatures [23]. It is also well known that the presence of sulfur containing compounds like polar-aromatics can deactivate the catalyst by strong bonding between sulfur and metallic sites [33]. As thus, once the metal sites were deactivated, its function is not capable of transforming aromatics to the compounds that are more reactive for cracking. Finally, the high temperature used (350°C) and the high amount of acid sites of nickel sample (Table 8.1) might also be responsible for the favorable formation of aromatics.

8.6. Conclusions

The catalytic pyrolysis of waste tire using bimetallic RuNi/HMOR catalysts prepared by successive impregnation technique has been investigated. The results showed strong influences of catalysts on the yield and nature of pyrolysis products and the catalytic activity depended on the metal composition α.

Significant synergistic effects of the catalysts were observed on both aromatic reduction and naphtha production in the tire-derived oil. And the synergy factor ζ was found to strongly depend on the metal composition of the catalysts, α (α = Ru/(Ru+Ni)). And ζ first increased with increasing α, reached a maximum at α = 0.36, and then decreased with further increasing α. Catalyst characterization results indicated that the close interaction between ruthenium and nickel, leading to the formation of bimetallic RuNi particles, was the cause for the observed synergistic effects. The stronger the interaction between ruthenium and nickel, the greater synergistic effect was obtained.

8.7 Acknowledgements

The Center of Excellence for Petroleum, Petrochemicals, and Advanced Materials, Chulalongkorn University, Thailand Research Fund (TRF), Office of Commission on Higher Education, and The Graduate Scholarship Program for Faculty Members from Neighboring Countries, Chulalongkorn University are acknowledged for their mutual financial support.

8.8 References

[1]. P.T. Williams and A.J. Brindle, J. Anal. Appl. Pyrolysis 67 (2003) 143-164

[2]. B. Benallal, C. Roy, H. Pakdel, S. Chabot, M.A. Poirier, Fuel 74 (1995) 1589-1594

[3]. Nguyễn Anh Dũng, Sujitra Wongkasemjit, Sirirat Jitkarnka, Catalytic pyrolysis of waste tire with noble metals-loaded HMOR catalysts, Manuscript Submitted to J. Anal. Appl. Pyrolysis.

[4]. A. Runez, A. De Lucas, L. Sanchez, M. J. Ramos, J.L. Valverde, Chemical Engineering Journal. 136 (2008) 267-275

[5]. J.H. Sinfelt, Bimetallic Catalysts: Discovery, Concepts and Applications, Wiley, New York, 1983.

[6]. V. Ponec, G.C. Bond, Catalysis by Metals and Alloys, Elsevier, Amsterdam, 1995

[7]. P.C. Das, N.C. Pradhan, A.K. Dalai, N.N. Bakhshi, Fuel. Process. Techno. 85 (2004) 1487-1501

[8]. C. Crisafulli, S. Scire, S. Minico, L. Solarino, Appl. Catal. A: Gen. 225 (2002) 1 -9.

[9]. M. Cerro-Alarcon, A. Guerrero-Ruiz, I. Rodriguez-Ramos, Catal. Today. 93-95 (2004) 395-403.

[10]. V.M. Akhemov, S.H. Al-Khowaiter, Appl. Catal. A: Gen. 197 (2000) 201-212

[11]. D. Li, M. Shiraga, I. Atake, T. Shishido, Y. Oumi, T. Sano, K. Takehira, Appl. Catal A: Gen. 321 (2007) 155-164

[12]. N.A. Dũng, A. Mhodmonthin, S. Wongkasemjit, and S. Jitkarnka, J. Anal. Appl. Pyro. 85 (2009) 338-344.

[13]. G. Sebor, J. Blaz ek, M.F. Nemer, J. Chromatogr A, 847 (1999), 323

[14]. E. Asedegbega-Nieto, B. Bachiller-Baeza, A. Guerrero-Ruiz, I. Rodriguez-Ramos, Appl. Catal. A: Gen. 300 (2006) 120-129.

[15]. M. Cerro-Alarcon, A. Guerrero-Ruiz, I. Rodriguez-Ramos, Catal. Today.

93-95 (2004) 395-403.

[16]. A. Guevara-Lara, R. Bacaud, M. Vrinat, Appl. Catal. A: Gen. 328 (2007) 99-108.

[17]. F. Iova, A. Trutia, Opt. Mater. 13 (2000) 455-458.

[18]. M.L. Jocono, M. Schavello, A. Cimino, J. Phys. Chem. 75 (1971) 1044-1050.

[19]. C.H. Bartholomew, R. B. Pannell, J. Catal. 65 (1980) 390.

[20]. D. Eliche-Quesada, J.M. Merida-Robles, E. Rodringuez-Castallon, A. Jimenez-Lopez, Appl. Catal. B: Environ. 65 (2006) 118.

[21]. A.S. Escobar, M.M. Pareira, H.S. Cerqueira, Appl. Catal. A: Gen. 339 (2008) 61-67.

[22]. K.A. Cumming, B.W. Wojciechowski, Catal. Rev. Sci. Eng. 38 (1996) 101.

[23]. A.W. Chester, Ind. Eng. Chem. Res. 26 (1987) 863.

[24]. Nguyễn Anh Dũng, Sujitra Wongkasemjit, Sirirat Jitkarnka, Roles of ruthenium and its particle size on the catalytic pyrolysis of waste tire, Manuscript submiited to Appl. Catal. B: Environ.

[25]. I. Eswaramoorthi, A. Geetha Bhavani, and N. Lingappan, Appl. Catal. A: Gen. 253 (2003) 469-486.

[26]. Nguyễn Anh Dũng, Sujitra Wongkasemjit, Sirirat Jitkarnka, Influences of pyrolysis temperature and Pt-loaded catalysts on the polar-aromatic content in tire-derived oils, Appl. Catal. B: Environ. In Press DOI:10.1016/j.apcatb.2009.05.038

[27]. E. Rodriguez-Castellon, J. Merida-Robles, L. Diaz, p. Maireles-Torres, J.J. Jones, J. Roziere, A. Jemenez-Lopez, Appl. Catal. A: Gen. 260 (2004) 9-18

[28]. N. Escalona, J. Ojeda, P. Baeza, R. Garcia, J.M. Palacios, J.L.G. Fierro, A. Lopez Agudo, and F.J. Gil-Llambias, Appl. Catal. A: Gen. 287 (2005) 47-53

[29]. S. Boxiong, W. Chunfei, G. Binbin, W. Rui, Liangcai, Appl. Catal. B: Environ. 73 (2007) 150-157

[30]. B.I. mosqueda-Jimenez, A. Jentys, K. Seshan, J.A. Lercher, J. Catal. 218

(2003) 348-353.

[31]. B.I. mosqueda-Jimenez, A. Jentys, K. Seshan, J.A. Lercher, J. Catal. 218 (2003) 375-385.

[32]. Eliche-Quesada, J.M Merida-Robles, E. Rodríguez-Castellon, A. Jiménez-Lopez, Appl. Catal. A: Gen. 279 (2005) 209-221

[33]. C. Naccache, M. Primet, M.V. Mathieu, J. Catal. 121 (1973) 266

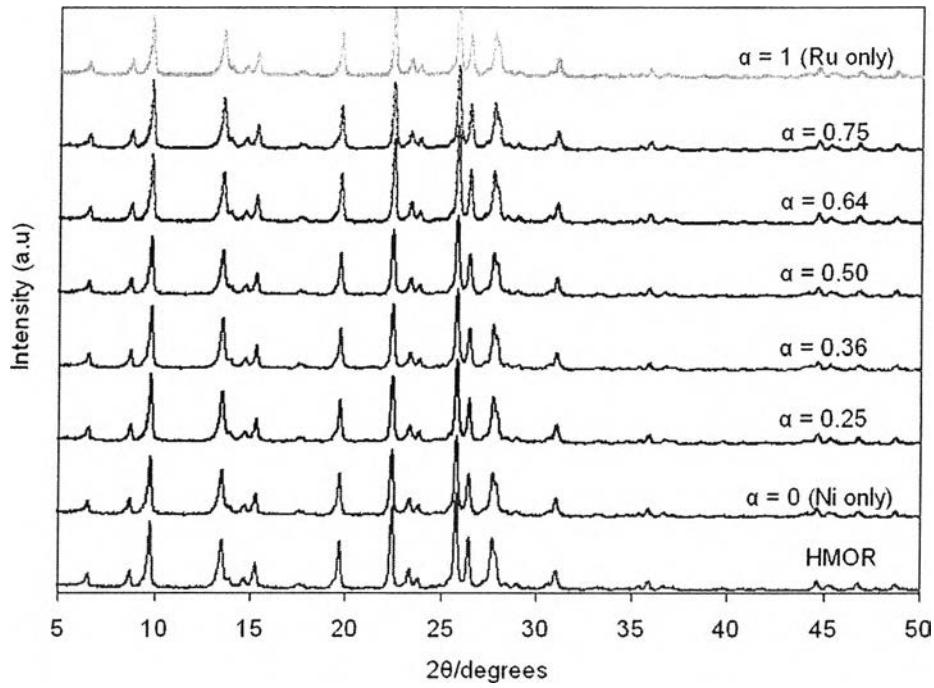

Figure 8.1 XRD patterns of RuNi/HMOR catalysts.

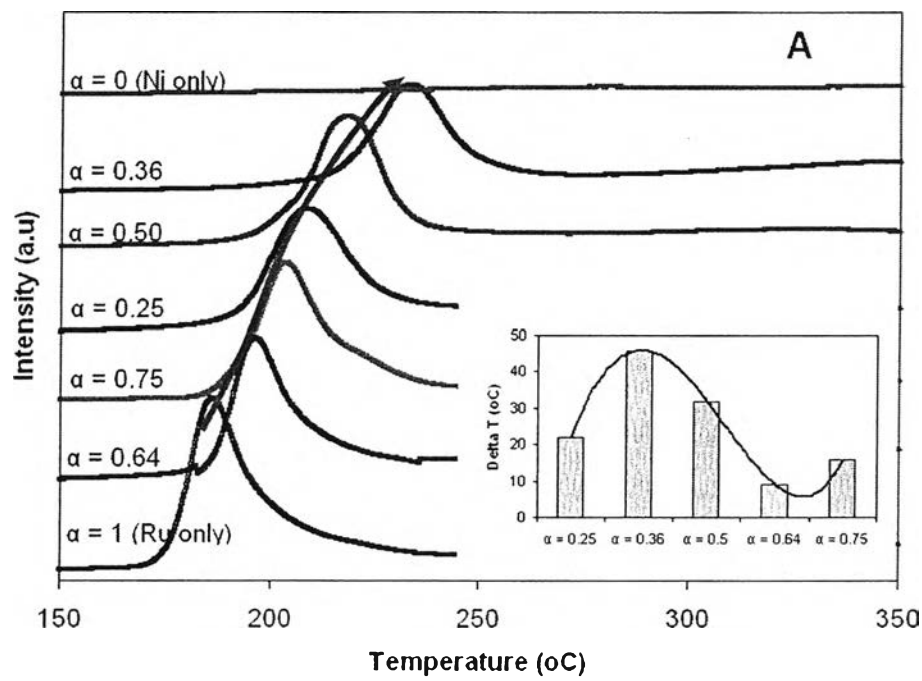

Figure 8.2A TPR profiles of metal-supported catalysts.

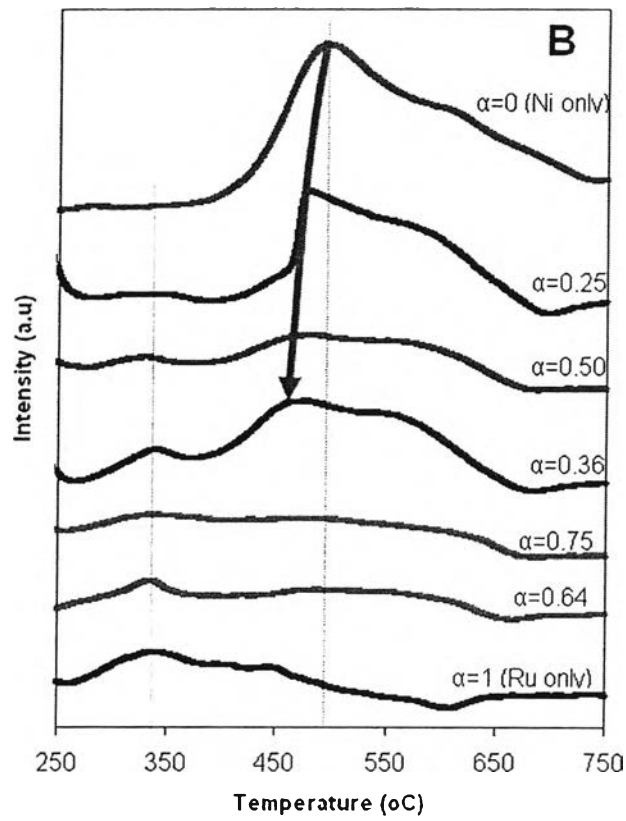

Figure 8.2B TPR profiles of metal-supported catalysts.

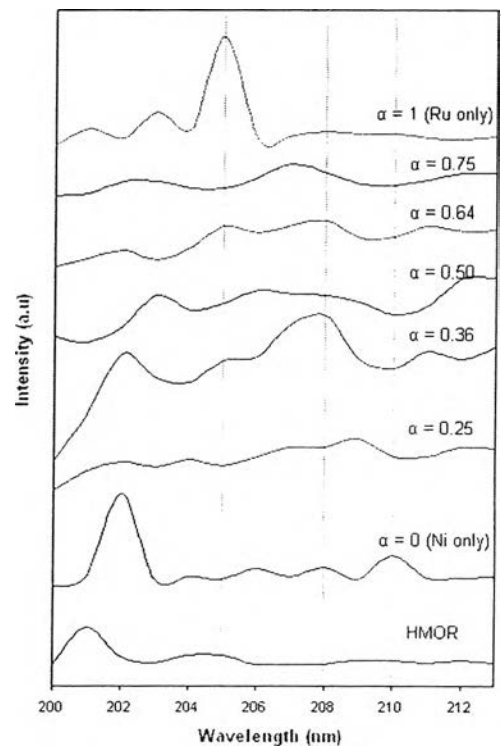

Figure 8.3 DRUV spectra of metal-supported catalysts.

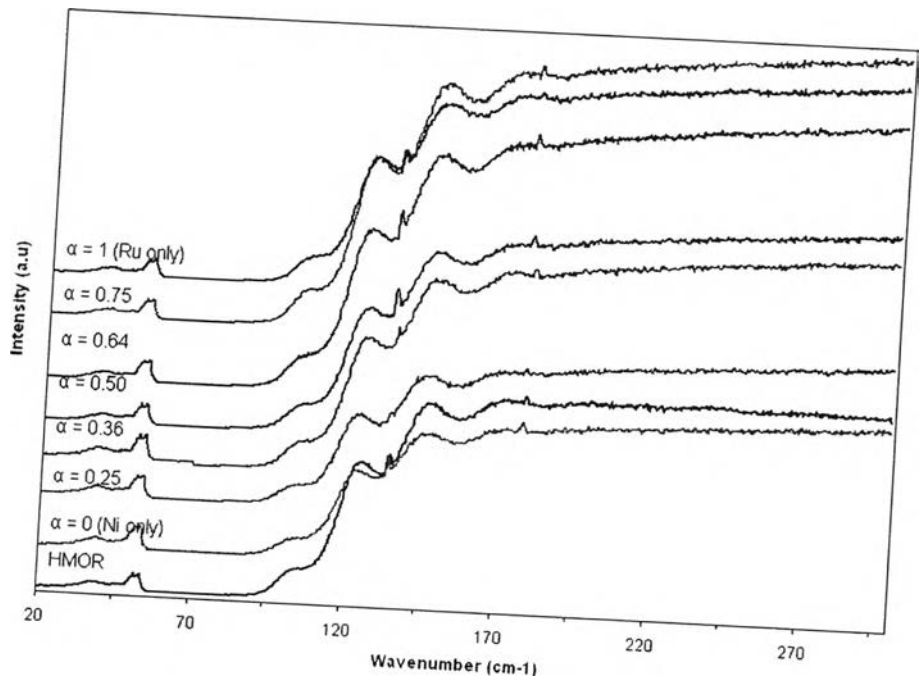

Figure 8.4 Raman spectra of metal-supported catalysts.

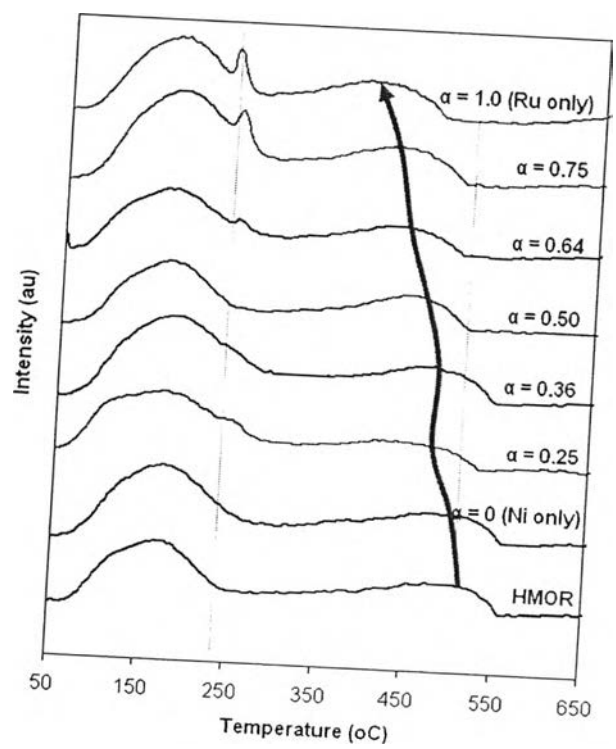

Figure 8. 5 TPD-NH_3 profiles of metal-supported catalysts.

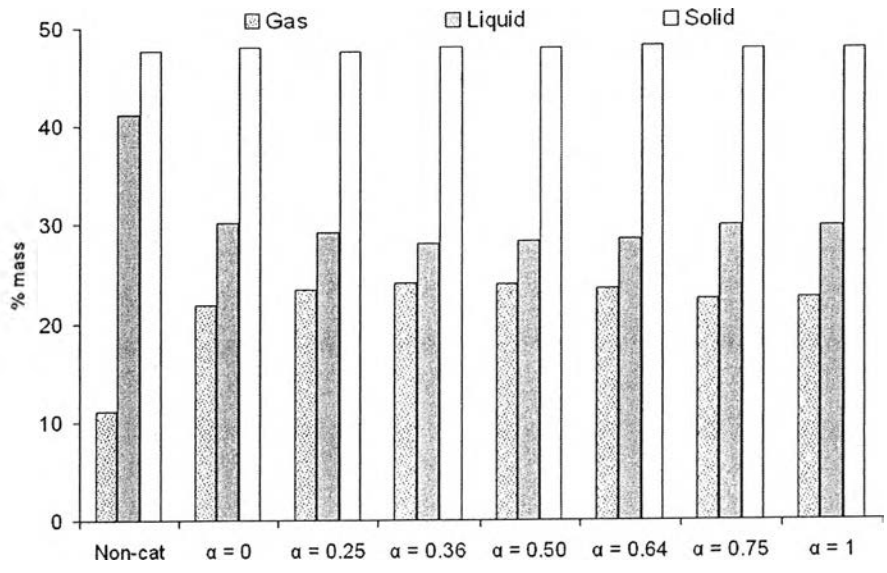

Figure 8.6 Yields (%wt) of pyrolysis products.

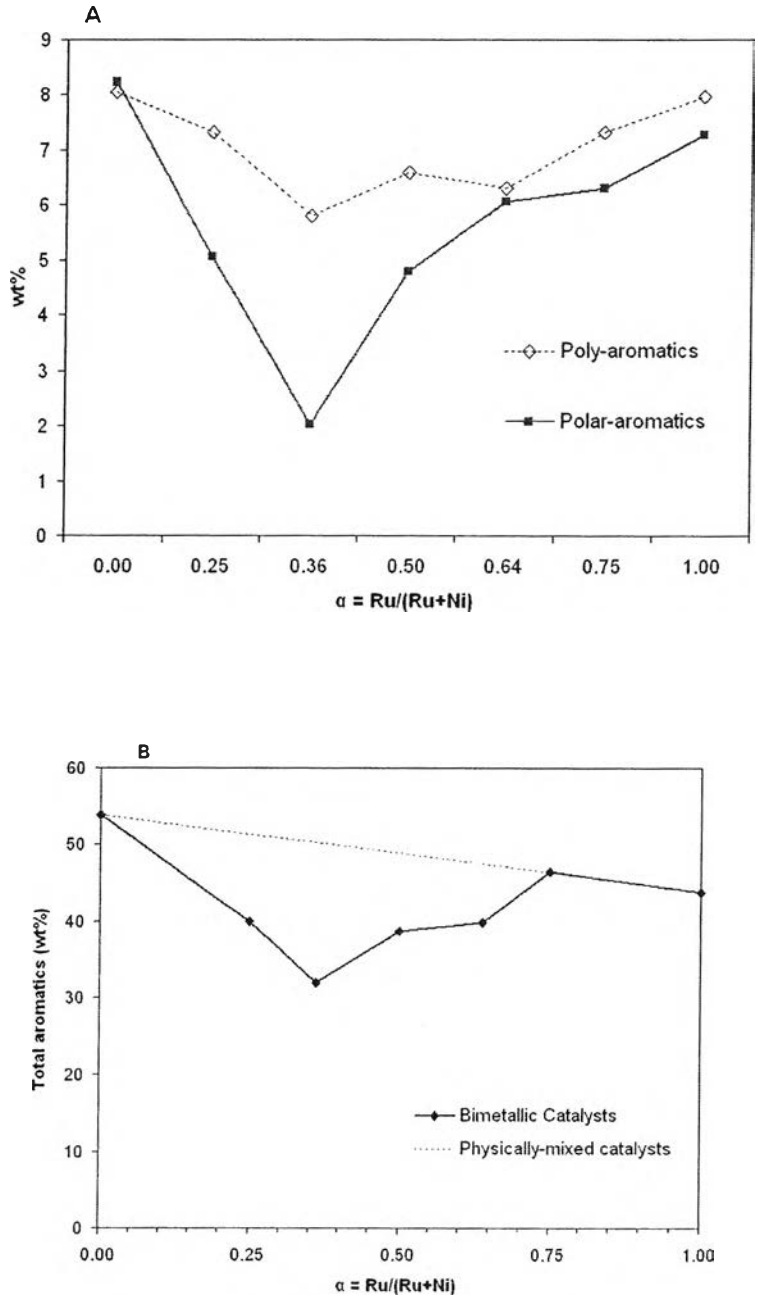

Figure 8.7 (A) Poly-, Polar-aromatics in oils, (B) Total aromatics in oils.

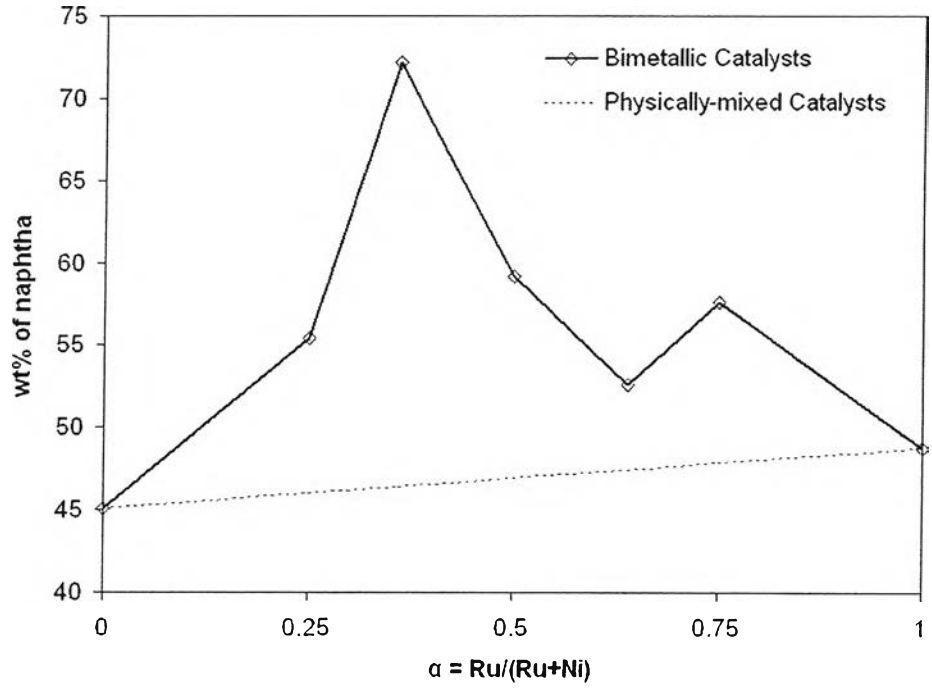

Figure 8.8 Naphtha content in tire-derived oils from using RuNi/HMOR catalysts.